AN ABSTRACT OF THE THESIS OF

Lydia I. Tai for the degree of Master of Science in Radiation Health Physics presented on October 26, 2016.

Title: Use of CR-39 for Nuclear Criticality Accident Dosimetry and High Neutron Dose Monitoring.

Abstract approved:

_____

David M. Hamby

CR-39 foils were irradiated as part of nuclear accident dosimetry experiments using the Godiva reactor at the Nevada National Security Site and the Caliban and Prospero reactors at the Valduc Centre for Nuclear Studies in France. The irradiated foils were chemically etched using the standard Lawrence Livermore National Laboratory process for personnel neutron dosimeters. Following chemical processing, the optical density of the CR-39 foils was measured using a transmission densitometer and found to be a function of the fast neutron dose as measured by the neutron activation components of the nuclear accident dosimeters. The relationship between fast neutron absorbed dose and optical density exponentially approaches a maximum at an absorbed dose of about 1 Gy. For the chemical etching process used in this study, neutron doses above 1 Gy did not further increase the optical density of the CR-39 foils.

Use of CR-39 for Nuclear Criticality Accident Dosimetry and High Neutron Dose Monitoring

by
Lydia I. Tai

A THESIS

submitted to

Oregon State University

in partial fulfillment of
the requirements for the
degree of

Master of Science

Presented October 26, 2016
Commencement June 2017

Master of Science thesis of Lydia I. Tai presented on October 26, 2016.

APPROVED:

_____

Major Professor, representing Radiation Health Physics

_____

Head of the School of Nuclear Science and Engineering

_____

Dean of the Graduate School

I understand that my thesis will become part of the permanent collection of Oregon State University libraries. My signature below authorizes release of my thesis to any reader upon request.

_____

Lydia I. Tai, Author

ACKNOWLEDGEMENTS

I would like to express my sincere appreciation for my colleagues at Lawrence Livermore National Laboratory who assisted me in completing this project. This work would not have been possible without the many contributions of those involved in the personnel dosimetry and nuclear accident dosimetry organizations, in particular Jack Topper, who provided both initial inspiration and continuous encouragement, and Debbie Madden, who generously shared her expertise with the CR-39 dosimetry program and personally etched nearly 500 CR-39 dosimeters that were used in this work.

I am especially indebted to Dr. David Hickman, who served as my on-site thesis advisor to provide detailed guidance, and to Dr. David Hamby, who provided long-distance support from Oregon State University. I am also truly grateful to Dr. David Heinrichs, Division Leader for the LLNL Criticality Safety Division, for his sustained interest in this project and its potential to be useful to the nuclear accident dosimetry program at LLNL.

Lastly, I am so thankful to my parents for being my constant supporters and cheerleaders throughout my graduate studies, to my sister Minna for setting the example and being a sage voice of wisdom, and finally to my husband Andrew for his tireless encouragement throughout this whole endeavor.

TABLE OF CONTENTS

LIST OF FIGURES

LIST OF TABLES

LIST OF ABBREVIATIONS

ANSI	American National Standards Institute
CEA	Commissariat à lénergie atomique et aux énergies alternatives (Alternative Energies and Atomic Energy Commission)
CFR	Code of Federal Regulations
CR-39	Columbia Resin #39
DOP	dioctyl phthalate
HPS	Health Physics Society
ICRP	International Commission on Radiological Protection
LLNL	Lawrence Livermore National Laboratory
NCERC	National Criticality Experiments Research Center
OD	optical density
PADC	poly allyl diglycol carbonate
PNAD	personnel nuclear accident dosimeter
TASL	Track Analysis Systems Ltd
TLD	thermoluminescent dosimeter

1 INTRODUCTION

1.1 NEUTRON DETECTION USING THE TRACK ETCH METHOD

Since neutrons cannot be detected directly, one method of indirect neutron detection is through the charged recoil particles they produce in interactions with matter. In solid state track-etch detectors, a charged recoil particle from a neutron interaction will cause radiation damage along its path in the detector material. Chemical or electrochemical etching techniques can be used on the detector material to enlarge the radiation damage sites and enhance their visibility (Turner 2007). Track-etch dosimeters exhibit an inherent threshold, since the specific energy loss ($-dE/dx$) of the charged recoil particle must be large enough to cause enough damage to lead to tracks that can be enhanced by the etching process. Thus, track-etch materials will be inherently insensitive to fast electron or gamma ray interactions (Knoll 2000).

CR-39 (poly allyl diglycol carbonate or PADC, with chemical formula $C_{12}H_{18}O_7n$) is one material widely used in solid state track-etch neutron dosimetry (Pinfold 2012). The chemical composition is close to that of human soft tissue, making it a roughly tissue equivalent detector (Sahoo 2015). Unirradiated CR-39 plastic has excellent optical properties and retains its clarity even after chemical etching. When irradiated with intermediate and fast neutrons, the latent damage caused by recoil particles is enhanced after chemical etching and degrades the optical properties of the CR-39 (Arneja 1995). CR-39 exhibits insensitivity to thermal neutrons and has a reaction threshold of about 100 keV (Hankins 1989).

1.1.1 NEUTRON DOSIMETRY AT THE LAWRENCE LIVERMORE NATIONAL LABORATORY

Routine neutron dosimetry at the Lawrence Livermore National Laboratory (LLNL) is conducted using the TASL system (Track Analysis Systems Ltd, Bristol, U.K.) with CR-39 plastic foils. Radiological workers at LLNL with the potential for exposure to neutrons are assigned a CR-39 dosimeter in addition to a Panasonic (Panasonic Industrial

Devices Sales Company of America, Newark, New Jersey) UD-802 or UD-810 thermoluminescent dosimeter (TLD) for beta and gamma dosimetry. A custom-designed and manufactured plastic case is used to hold both components, along with shielding for specific TLD elements. A disassembled view of the LLNL personnel dosimeter package is pictured in Figure 1.

Figure 1. LLNL Dosimeter Case with Panasonic UD-810 and CR-39 Foil

When dosimeters are returned to the LLNL External Dosimetry Laboratory for reading, the CR-39 foil is processed using a chemical etching procedure to enlarge the latent tracks created by neutron-induced recoil particles. For routine personnel dosimetry, the tracks are counted using the TASL system, which uses Nikon optics for transmitted light microscopy and automated track analysis using the TASL*IMAGE* software. The software analyzes each microscope image to measure and account for track characteristics,

including length, diameter, position, and symmetry. Through these analyses, the software is able to discriminate neutron tracks from background features (Topper 2016).

1.1.2 LIMITATIONS OF THE TASL SYSTEM

The TASL system has been tested for linearity of neutron dose response using an unmoderated ^{252}Cf source in the LLNL Radiation Calibration Laboratory. The TASL system was shown to be linear through 300 mSv and became non-linear between 300–500 mSv. The average track density for a 300 mSv neutron exposure exceeded 1.5×10^5 tracks cm^{-2}, and the average track density for the 500 mSv neutron exposure exceeded 1.3×10^6 tracks cm^{-2} (Topper 2016). These effective dose values were determined using measured neutron energy spectra and the fluence-to-dose conversion factors for personal dose equivalent $H_p(10,0)$ as defined in ICRP Publication 74 (ICRP 1996). Based on these previously reported conversion factors for the unmoderated ^{252}Cf source, 500 mSv is equivalent to about 34 mGy (Radev 2009). Thus, it is apparent that the TASL track analysis method is not usable for very high neutron absorbed doses between 0.1 to 10 Gy, such as those that could take place in a criticality accident.

1.2 DOSIMETRY REQUIREMENTS FOR CRITICALITY ACCIDENTS

Title 10, Part 835 of the Code of Federal Regulations (CFR) requires Department of Energy facilities with sufficient fissile material such that "excessive exposure of individuals to radiation from a nuclear accident is possible" to provide nuclear accident dosimetry for those individuals. Further, Section 835.1304 requires such a nuclear accident dosimetry program to include the following four components: (1) a method for initial screening of individuals to determine whether significant exposures occurred, (2) methods and equipment for analysis of biological materials, (3) a system of fixed nuclear accident dosimeters, and (4) personal nuclear accident dosimeters (10 C.F.R. § 835, 2016). The American National Standards Institute and the Health Physics Society (ANSI/HPS) Standard N13.3-2013, *Dosimetry for Criticality Accidents,* provides

requirements and performance criteria for a dosimetry system capable of providing personal absorbed doses in the event of a criticality accident.

1.3 NUCLEAR ACCIDENT DOSIMETRY AT LLNL

Nuclear accident dosimeters are issued to LLNL employees who work in facilities where a criticality accident is considered credible. The LLNL Personnel Nuclear Accident Dosimeter (PNAD) design was first developed in the 1980s and its current configuration is illustrated in Figure 2. The LLNL PNAD incorporates six neutron activation elements and a Panasonic UD-810 thermoluminescent dosimeter (TLD). The neutron activation elements are sized to fit in the wells surrounding the Panasonic TLD in the standard LLNL dosimeter case. For LLNL employees who work full-time in a facility where routine exposure to neutrons and a criticality accident are both possible, a CR-39 foil is also included to monitor routine neutron dose. This work was undertaken to determine the feasibility of using the CR-39 foil to provide accident-level neutron dose data in addition to those provided by the neutron activation elements of the PNAD.

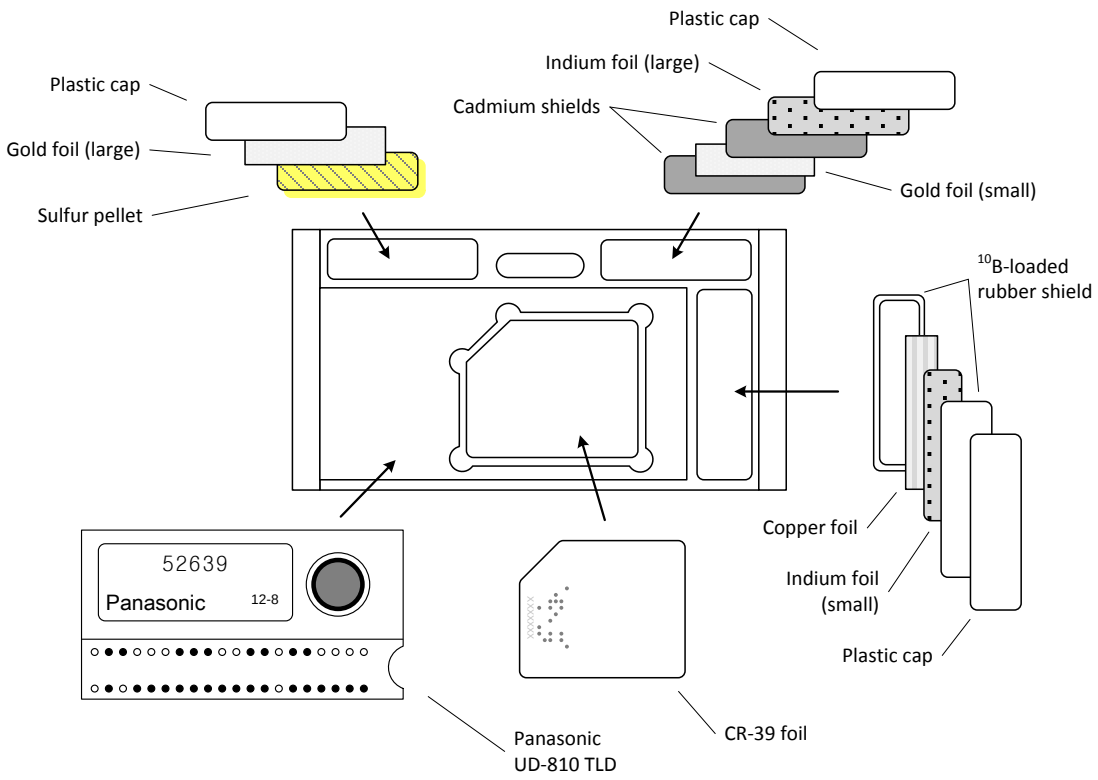

Figure 2. Components of LLNL Personnel Nuclear Accident Dosimeters

1.3.1 NEUTRON ACTIVATION ELEMENTS OF THE LLNL PNAD

The neutron activation elements of the LLNL PNAD and their energy thresholds for activation are given in Table 1, along with the neutron activation reaction that takes place. Five metal foils with various shields and a sulfur pellet comprise the LLNL PNAD. Since the calculations for determining neutron fluence from the activated elements use measured activity concentration (activity per mass), stringent specifications for dimensions or mass of the metal foils and the sulfur pellet are not necessary. The elements do need to meet size limitations and must fit within the specified compartments of the dosimeter case illustrated in Figure 2. The average foil dimensions and masses of the LLNL PNAD components are provided in Table 2. With additional information determined by using the specified shielding materials, the activation elements are used to resolve the neutron spectrum through neutron activation analysis (LLNL 2012).

Table 1. Neutron Activation Elements of the LLNL PNAD

Activation Element	Shielding	Reaction	Threshold Energy
Gold	Cadmium	^{197}Au (n, γ) ^{198}Au	0.025 eV
Copper	Borated rubber	^{63}Cu (n, γ) ^{64}Cu	1 eV
Indium	Borated rubber	^{115}In (n, n′) ^{115m}In	0.5 MeV
Sulfur	None	^{32}S (n, p) ^{32}P	3 MeV

Table 2. Average LLNL PNAD Metrics

Activation Element	Mass (g)	Length[1] (mm)	Width (mm)	Thickness (mm)
Gold (shielded)	0.208 ± 0.007	17.94 ± 1.56	4.57 ± 0.46	0.15 ± 0.03
Gold (bare)	0.281 ± 0.009	20.67 ± 0.30	6.05 ± 0.06	0.15 ± 0.02
Copper	0.474 ± 0.009	16.34 ± 0.12	3.75 ± 0.08	0.65 ± 0.02
Indium (shielded)	0.362 ± 0.007	19.13 ± 0.48	4.66 ± 0.14	0.62 ± 0.05
Indium (bare)	0.517 ± 0.006	20.78 ± 0.33	5.96 ± 0.56	0.61 ± 0.04
Sulfur	0.867 ± 0.023	20.7[2]	5.6	4.0

Two gold foils are used in the LLNL PNAD. The larger of the two foils is unshielded, while the smaller foil is surrounded by cadmium. The radiative capture cross section for cadmium is very large for neutron energies below about 0.4 eV and then drops abruptly for higher neutron energies (Knoll 2000). Thus, cadmium is used as a shield for one of the gold foils to absorb the thermal portion of the neutron fluence.

The difference in mass activation for the two gold foils yields the thermal component of the total neutron fluence. This arrangement allows for the removal of epithermal and higher-energy neutrons and resonance absorption influences on the thermal neutron component. Since the fluence of thermal neutrons in a fission event is relatively low, the difference in size between the two foils allows for improved mathematical certainty and accuracy in determining the difference in activity concentration in the shielded versus unshielded gold foils. However, too small of a shielded gold piece will reduce sensitivity for measuring thermal neutron fluence (LLNL 2012).

[1] The average measurements for length, width, and thickness are from the Technical Basis for the LLNL Nuclear Criticality Accident System (LLNL 2012). The average masses are specific to the PNADs used in this work.
[2] Based on a single measurement.

The copper foil is surrounded by a ^{10}B-loaded rubber shield, which also absorbs the thermal portion of the neutron fluence. Unlike cadmium, borated rubber does not interact chemically with the indium or copper foils, and the cross-section for neutrons in the range of 0.5 eV to 1 keV is significantly higher for ^{10}B than it is for cadmium, greatly reducing the overresponse of the copper foil at low neutron energies (Griffith 1973). This shield is composed of 82% (by weight) enriched ^{10}B, with the remainder consisting of a rubber binder. The neutron activation results of the copper foil are used to determine the epithermal and intermediate portion of the neutron fluence (1 eV to 1 MeV) (LLNL 2012). For simplicity, this energy range will be referred to as the "intermediate" neutron energy range throughout this work.

The smaller of the two indium foils is also placed inside the ^{10}B-loaded rubber shield, in front of the copper foil (away from the wearer). The threshold for the ^{115}In (n, n′) ^{115m}In reaction is approximately 0.35 MeV and the resulting ^{115m}In can be further activated to ^{116m}In by thermal neutrons. The design of the LLNL PNAD minimizes the thermal neutron interaction by placing the smaller indium foil within the ^{10}B-loaded rubber shield. The results of the smaller indium foil are used to determine the fluence for fast neutrons (>1 MeV) (LLNL 2012).

The larger of the two indium foils is used as a means for rapid identification ("quick sort") of personnel who received the most significant doses in a criticality accident. It can be used as a backup to the ^{115m}In measurement for determining the fluence for fast neutrons (>1 MeV) once the shorter-lived ^{116m}In has decayed significantly. If counted twice (once soon after irradiation, and again after the ^{116m}In has decayed), it can also be used as a backup to the thermal neutron fluence determination (LLNL 2012).

The unshielded sulfur pellet is used to determine the fluence for fast neutrons (>3 MeV). The cross section for the ^{32}S (n, p) ^{32}P reaction has a threshold of about 3 MeV. Unlike the gold, indium, and copper foils which are analyzed using gamma spectroscopy, the

sulfur pellets are counted whole for beta activity from the resulting ^{32}P using a Canberra (Canberra Industries, Inc., Meriden, Connecticut) iSolo® Alpha/Beta Counting System.

1.3.2 NEUTRON DOSE DETERMINATION

In order to calculate external doses, a set of conversion coefficients must be used to relate basic physical quantities to radiological protection quantities (ICRP 1996). The physical quantities relevant to this work are *fluence* (*Φ*) and *tissue absorbed dose* (*D*). In the context of criticality accident dosimetry, absorbed dose is the appropriate quantity instead of the radiological protection quantity *effective dose* (*E*), since absorbed dose is applicable to an acute dose potentially resulting in immediate nonstochastic effects (ANSI/HPS 2013). Absorbed dose is defined in terms of dε, the mean energy imparted by ionizing radiation, and dm, the mass of irradiated matter. The unit of absorbed dose is joule per kilogram, which is given the special name of gray (Gy).

$$D = \frac{\mathrm{d}\varepsilon}{\mathrm{d}m} \qquad \text{Equation 1}$$

Fluence *(Φ)* is defined as the quotient of dN by da, where dN is the number of particles incident on a sphere of cross-sectional area da (ICRP 1996). In the LLNL PNAD design, the decay-corrected activity concentrations (activity per mass) of the components are converted to neutron fluence using experimentally derived conversion coefficients (LLNL 2012). The calculated neutron fluence can then be converted to tissue absorbed dose by use of another set of conversion coefficients that depend on the neutron energy range. The LLNL Technical Basis Document (LLNL 2012) uses fluence-to-dose conversion coefficients derived for Element 57 of the cylindrical phantom as described by Auxier, Snyder, and Jones (Hankins 1984, Auxier 1968).

1.4 PREVIOUS WORK INVESTIGATING CR-39 AS A DOSIMETER FOR HIGH NEUTRON EXPOSURES

CR-39 has been studied extensively as a neutron dosimeter. For routine use in personnel dosimetry, individual tracks can be counted and analyzed as described in Section 1.1.1.

For high neutron doses, individual tracks cannot be counted due to overlap, and the high track density will cause the foil to become less transparent and take on a "frosted glass" appearance after chemical etching. The decrease in transparency can be quantified by measuring the optical density of the foil. Optical density is defined as the common logarithm of the ratio of light incident on the material to the light transmitted through it (Equation 2). A transmission densitometer determines the optical density of a material by comparing the intensity of a known light source to the light transmitted through a material.

$$\mathrm{OD} = \log_{10}\left(\frac{I_0}{I_i}\right) \qquad \text{Equation 2}$$

This technique has been previously investigated by Bordy et al. with irradiations of up to 100 Gy performed at the SILENE reactor in France. Light transmission through chemically etched CR-39 samples was measured using a spectrophotometer and found to be a linear function of dose to certain limits. The limits of linearity were found to be dependent on the etching time (Bordy 1991).

Similar investigations were performed by Arneja and Waker with neutron doses up to 10 Gy from a bare ^{252}Cf source. This study also used optical density measurements taken by spectrophotometry and included a comparison of monochromatic light sources. A light source with wavelength 500 nm was reported to have almost 100% transmission for unirradiated and unetched CR-39, providing the maximum potential to observe differences in optical density of irradiated foils (Arneja 1995).

Yasuda et al. have also studied the use of CR-39 for high neutron doses, but instead of measuring light transmission, atomic force microscopy was used to analyze the irradiated and etched foils. This method allows for the use of additional information regarding the shape of the etch pits, which assist in determining the charge of the recoil particle causing the tracks or their linear energy transfer. The etch pit density as measured by atomic force microscopy was found to be a linear function of dose to the maximum evaluated dose of 6 Sv (Yasuda 2006).

1.5 SCOPE OF THIS WORK

In this work, CR-39 foils routinely assigned to Lawrence Livermore National Laboratory radiation workers were evaluated for potential use in extremely high neutron dose situations, such as a criticality accident. The LLNL personnel nuclear accident dosimeters are built into the standard dosimeter case. Radiation workers expected to receive routine neutron exposures are assigned CR-39 dosimeters which are also built into the single dosimeter case. The current TASL system is not capable of analyzing the CR-39 foils in accident-level neutron exposures, so this work is intended to investigate the possibility of making use of the CR-39 foils in an accident scenario.

The LLNL personnel nuclear accident dosimeters are based on neutron activation elements, and the activation products with the shortest half-lives must be individually and rapidly analyzed by gamma spectroscopy. This time-consuming analysis means that nuclear accident dosimeters are expected to be used as a triage tool to prioritize medical attention and dosimetry analysis for the individuals with the highest apparent exposures. Other workers could have received measurable neutron exposures, but the activated dosimeter elements may decay significantly before they can be analyzed. In such cases, the CR-39 foils could serve as a valuable backup if they could be found to reliably indicate high neutron doses beyond the capability of the TASL track counting system.

CR-39 foils were included as integral components of LLNL PNADs and irradiated to accident-level absorbed doses between 0.1–5 Gy at the Godiva reactor at the Nevada National Security Site and the Caliban and Prospero reactors at the Valduc facility in France. The CR-39 foils were chemically etched using the standard etching procedure for personnel neutron dosimeters at LLNL. A simple and relatively inexpensive instrument for measuring optical density was desired for this study, so optical density was measured using a transmission densitometer.

2 MATERIALS AND METHODS

2.1 MATERIALS

The CR-39 foils used in this work were of dosimetry-grade CR-39 resin with 0.1% dioctyl phthalate (DOP) additive and were purchased from Intercast Europe S.r.l. (Parma, Italy). The size of each foil was 25 mm × 20 mm × 1.5 mm. During storage, dosimeter assembly, and irradiation, both sides of the foil were covered with clear polyethylene material of 0.5 mm nominal thickness to protect against abrasions and alpha particles resulting from the decay of radon and radon daughters. These protective coverings were removed just prior to the chemical etching process.

In addition to its protective function, the polyethylene covering also serves as a radiator for the CR-39 foils (Castillo 2013). The polyethylene has a greater hydrogen density than CR-39 and therefore generates more recoil protons from (n, p) reactions, contributing to the total number of interactions in the CR-39. For neutrons with energies higher than 1 MeV, the recoil protons from the polyethylene layer can reach the CR-39 and enhance its response by producing additional tracks. Below 1 MeV, the protons originating in the polyethylene layer either do not reach the CR-39 or have too little energy to damage the foil (Hankins 1989).

The CR-39 foils were included as components of standard LLNL PNADs. The neutron activation elements were analyzed after each irradiation as described in Section 3.1 below. The CR-39 foils were removed from the dosimeter case and shipped to LLNL for processing as described in Section 3.2 below.

2.2 SAMPLE IRRADIATION

2.2.1 IRRADIATIONS AT THE NEVADA NATIONAL SECURITY SITE

Three irradiations were performed in May 2014 as part of an international collaboration to characterize the Godiva IV fast burst reactor at the National Criticality Experiments Research Center (NCERC). Godiva IV is a bare cylindrical assembly of approximately

65 kg of highly enriched uranium fuel (93.2% ^{235}U metal alloyed with 1.5% molybdenum for strength) and is designed to perform controlled prompt critical excursions (Myers 2010, Goda 2013). Three irradiations were performed with fuel core temperature increases of 71.1°C, 136.9°C, and 229.9°C during the burst excursions and are referred to in this report as Godiva 70, Godiva 140, and Godiva 250 based on the target core temperatures.

CR-39 foils were included as components of four hundred thirty-two (432) LLNL PNADs deployed to evaluate the Godiva neutron field. In each irradiation, nine support stands with aluminum plates were placed at predetermined positions around the reactor core. The stand placement positions are illustrated in Figure 3.

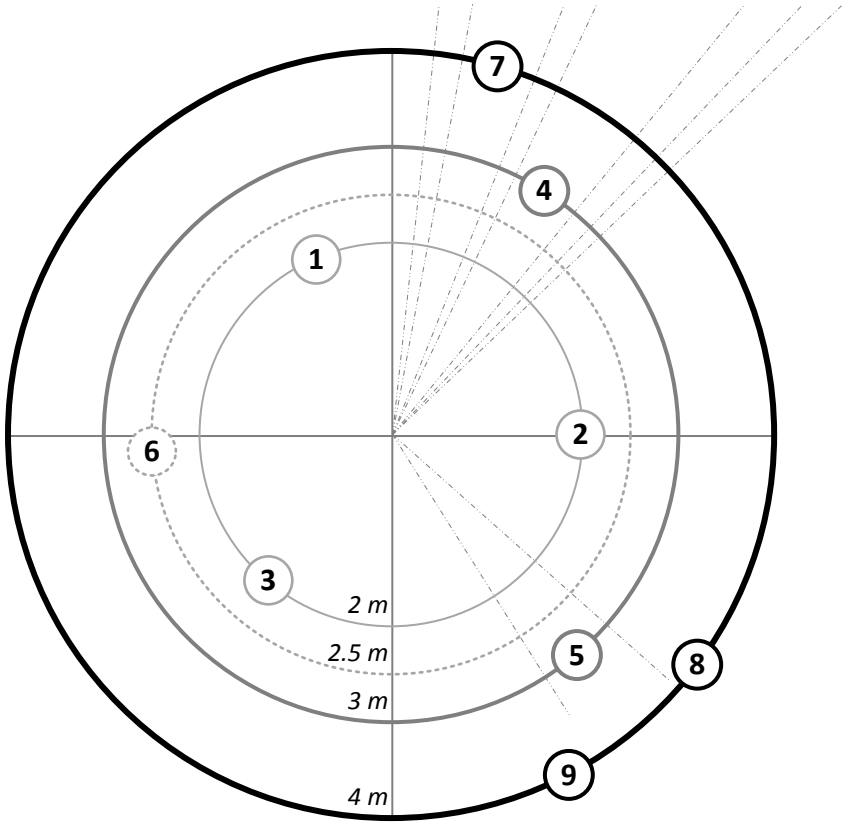

Figure 3. Placement of Dosimeters around Godiva

Each stand held four LLNL dosimeters at each of four different heights, as pictured in Figure 5. The height of the top of each aluminum plate is given in Table 3. The height of the Godiva core is 180 cm; thus, the effective distance between the row of dosimeters on each plate and the Godiva assembly core was calculated as illustrated in Figure 4 and is given in the last column of Table 3.

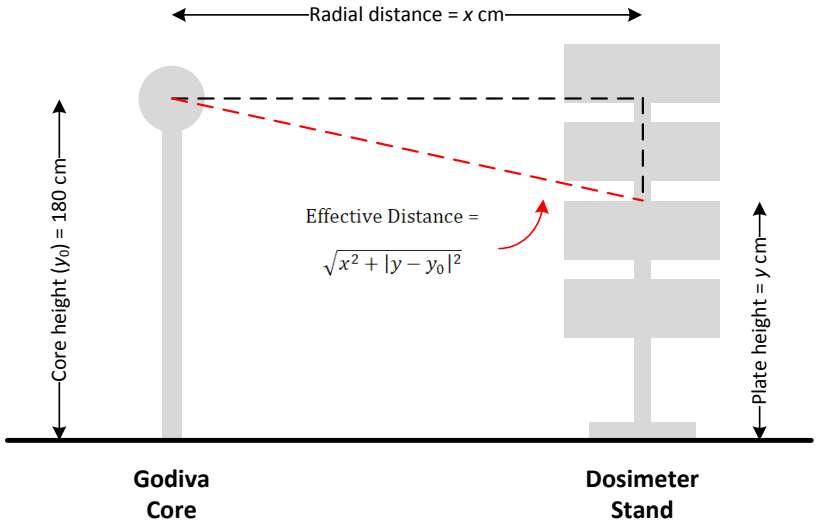

Figure 4. Calculation of Effective Distance between Reactor Core and Dosimeter

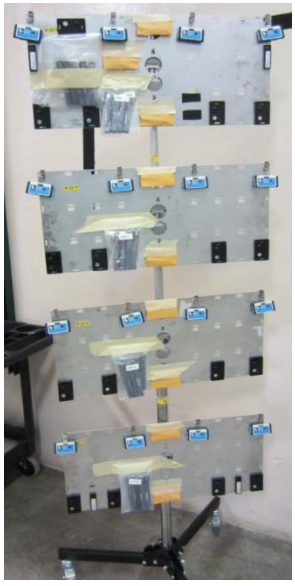

Figure 5. Aluminum Stand Used in the Godiva Irradiations

Table 3. Heights and Effective Distances of Dosimeter Holding Plates

Location	Radial Distance from Reactor Core (m)	Plate Identification	Top of Plate Height (cm)	Effective Distance from Core (cm)
1, 2, 3	2	AB	197	200.7
		CD	156	201.4
		EF	115	210.3
		GH	70.5	228.0
4, 5	3	AB	220	302.7
		CD	169.5	300.2
		EF	119.5	306.0
		GH	69	319.9
6	2.5	AB	220	253.2
		CD	169.5	250.2
		EF	119.5	257.2
		GH	69	273.5
7, 8, 9	4	AB	234	403.6
		CD	178.5	400.0
		EF	123	404.0
		GH	67.5	415.5

2.2.2 IRRADIATIONS AT THE CEA VALDUC FACILITY

Two irradiations were performed in September 2014 in collaboration with the French Commissariat à l'énergie atomique et aux énergies alternatives (Alternative Energies and Atomic Energy Commission, CEA). As in the Godiva irradiations, CR-39 foils were included as components of forty-one (41) LLNL PNADs that were irradiated at the CEA Valduc facility. Twenty-four (24) dosimeters were irradiated in a burst experiment using the Caliban reactor at a core burst temperature of 61.8°C and 17 dosimeters were irradiated at a steady state of 100 W for 1500 seconds using the Prospero reactor (Lobaugh 2015).

Caliban is a vertically oriented cylindrical reactor with highly enriched uranium fuel plates (93.5% ^{235}U alloyed with 10% in weight of molybdenum). Four control rods of the

same uranium alloy are used for reactor operation. Caliban can be operated in either a steady state power mode or a pulsed mode with a neutron fluence in the irradiation cavity of about 4×10^{14} n cm^{-2} (Casoli 2014). In the Caliban irradiation, dosimeters were placed on two phantoms and one aluminum stand. The stand and one phantom directly faced the reactor core, while the other phantom was arranged at a 45° angle. The radial distance of all dosimeter positions in the Caliban irradiation was 3 m from the reactor.

Figure 6 illustrates the dosimeter stand and phantom positions for the Caliban irradiation. LLNL PNADs were only placed at locations S1, P_2, and P_3. For consistency with the Godiva data, in which all PNADs were irradiated on direct-facing stands, only the Caliban data for Stand S1 are presented in this work.

Figure 7 depicts the stand setup for the Caliban irradiation. The heights of each set of dosimeters are indicated in the figure. The height of the Caliban reactor is 25 cm and the effective distance from the reactor to the dosimeters was calculated in the same manner as for the Godiva irradiations.

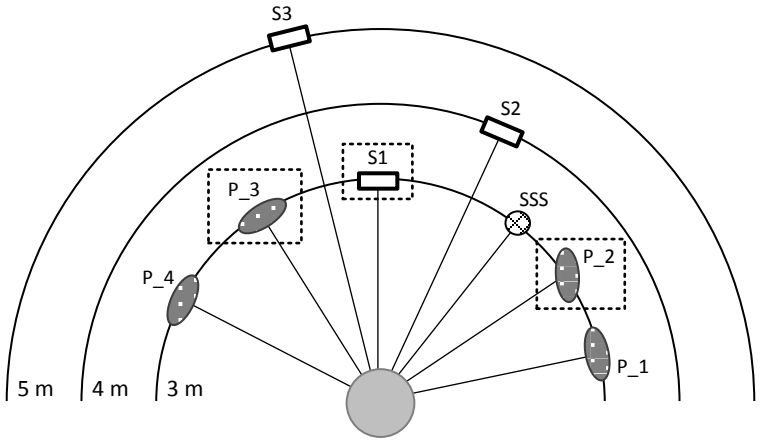

Figure 6. Placement of Dosimeters around Caliban

Figure 7. Stand S1 in the Caliban Irradiation

Prospero is also a metallic core cylindrical reactor, but is horizontally oriented. It is composed of metallic plates of a highly enriched uranium alloy surrounded by a depleted uranium and steel reflector. Four depleted uranium control rods in the reflector are used to operate the reactor. Prospero can only be operated in a steady state power mode (Casoli 2014). In the Prospero irradiation, dosimeters were again placed on two phantoms and one aluminum stand. The stand and one phantom directly faced the reactor core, while the other phantom was arranged at a 45° angle relative to the reactor. The radial distance of all dosimeter positions in the Prospero irradiation was 3.5 m from the reactor.

Figure 8 illustrates the dosimeter stand and phantom positions for the Prospero irradiation. LLNL PNADs were placed at all locations, but for experimental consistency, only the Prospero data for Stand S4 are presented in this work.

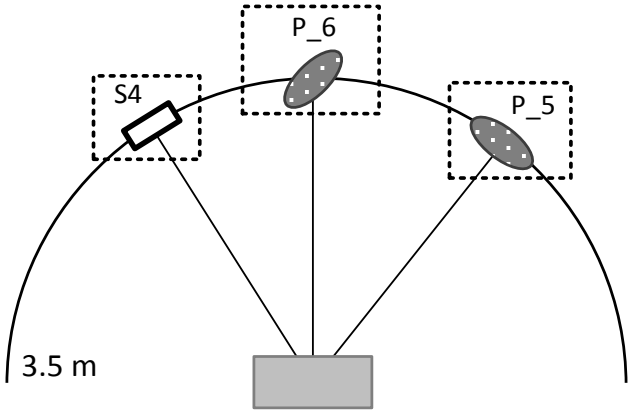

Figure 8. Placement of Dosimeters around Prospero

Figure 9 depicts the stand setup for the Prospero irradiation. The heights of each set of dosimeters are indicated in the figure. The height of the Prospero reactor is 35.3 cm and the effective distance from the reactor to the dosimeters was calculated in the same manner as for the Godiva irradiations.

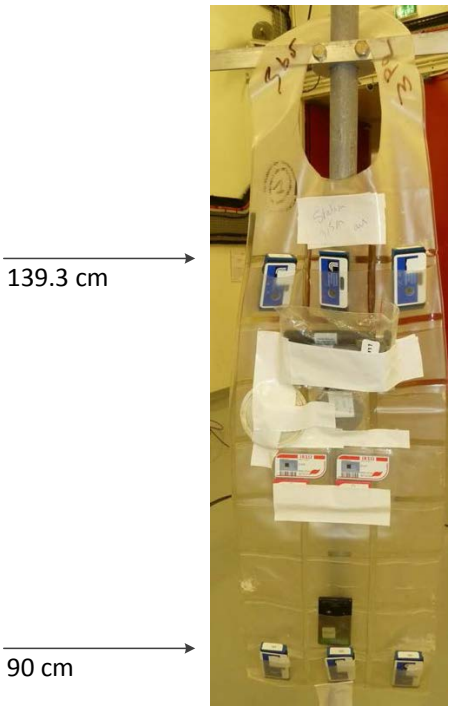

Figure 9. Stand S4 in the Prospero Irradiation

2.3 DOSIMETER PROCESSING

2.3.1 CHEMICAL ETCH

All CR-39 foils were chemically etched according to the LLNL procedure for personnel neutron dosimeters. This procedure is based on the TASL user manual but has been optimized for operations at LLNL, as described in the TASL CR-39 System Technical Basis Document (Topper 2016). The foils were chemically etched for 2 hours and 50 minutes in a 6.05 M NaOH bath heated to 85°C. The molarity (concentration in moles NaOH per liter solution) of the etch bath was verified to be slightly less than 6.05 M before beginning the heating process by using a refractometer.

Following the chemical etch, the foils were rinsed in three separate tanks. The first rinse lasts 15 minutes in a solution of acetic acid and water, while the second and third rinses lasted five minutes each in deionized water only. All three rinses used frequent agitation by hand during the rinse period. Following the three sequential neutralizing rinses, the foils were initially dried with nitrogen gas and then fully dried for a least one hour in the manufacturer-provided dryer.

A set of five blank and five reference foils were also processed and etched along with the sample foils. The blank foils were not irradiated, while the reference foils were irradiated with the bare ^{252}Cf source in the LLNL Radiation Calibration Laboratory to an absorbed dose of 0.34 mGy.

Immediately following the etching process, the CR-39 foils that were irradiated for this work had visible damage and obviously had sustained extensive neutron irradiation. The visual difference between the reference foils irradiated to 0.34 mGy and the Godiva foils, which were etched together in the same batch, is depicted in Figure 10.

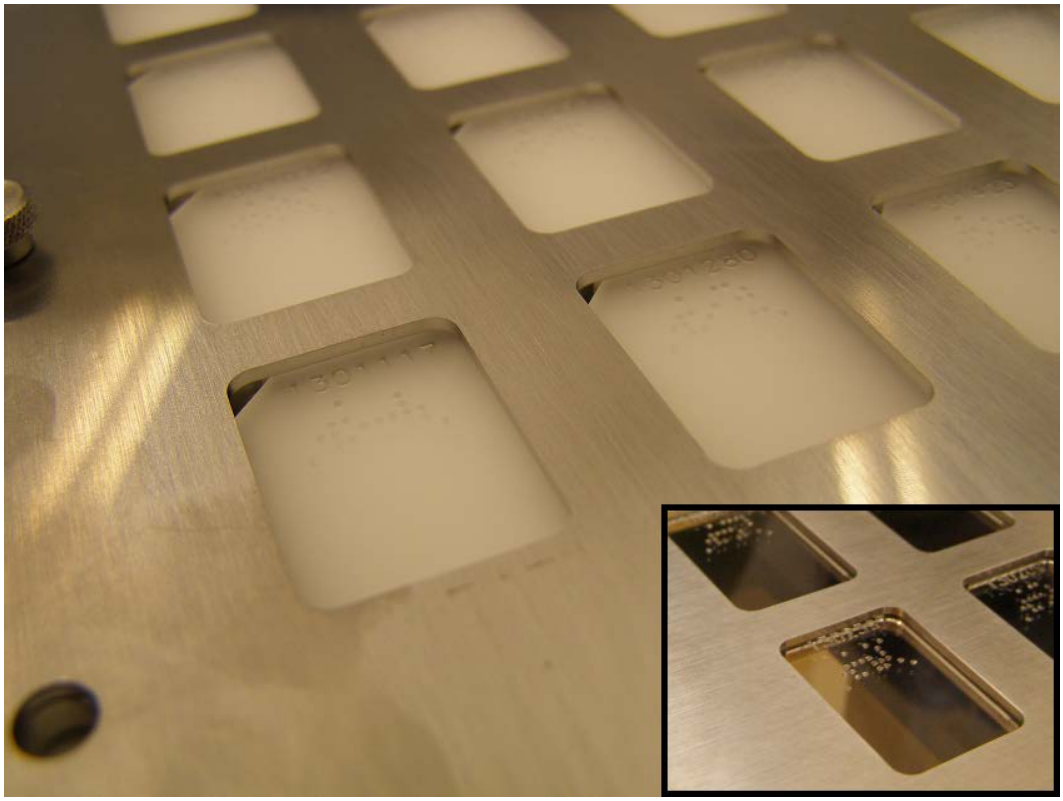

Figure 10. Visual Post-Etch Comparison of Foils Irradiated in Godiva 140 and Reference Foils Irradiated to 0.34 mGy (inset)

2.3.2 MEASUREMENT OF OPTICAL DENSITY

Following chemical etching, the optical density of the CR-39 foils was measured using an X-Rite 301 transmission densitometer (X-Rite, Incorporated, Grand Rapids, Michigan). Optical density measurements were taken near the center of each foil using the densitometer fitted with a standard 2 mm aperture provided by the manufacturer. Prior to each set of measurements, the calibration of the densitometer was checked using the calibration step tablet, also provided by the manufacturer. The optical density of the blank (unirradiated) and reference (irradiated to 0.34 mGy) foils were also measured with the transmission densitometer.

3 RESULTS

3.1 LLNL PNAD RESULTS

3.1.1 DETERMINATION OF NEUTRON FLUENCE

The distribution of neutron energies of each irradiation was determined by measurement of the activated PNAD elements. The neutron activation elements were analyzed soon after irradiation and decay-corrected to the irradiation time. The process is described in Section 1.3.1 and further detailed elsewhere (LLNL 2012).

Activity-to-fluence conversion coefficients given in the LLNL technical basis document (LLNL 2012) were used to determine the neutron fluence from the activity concentration measurements. These coefficients are reproduced in Table 4.

Table 4. Activity-to-Fluence Conversion Coefficients for LLNL PNAD Elements

Activation Element	Activity-to-Fluence Conversion Coefficient (n g cm^{-2} Bq^{-1})
Gold	8.11×10^{5}
Copper	1.35×10^{8}
Indium	1.84×10^{7}
Sulfur (whole pellet)	7.84×10^{8}

The results of neutron fluence for each irradiation are shown in the figures on the following pages. The results for the dosimeters on each stand were averaged in groups according to their effective distance from the reactor core. Detailed results of the PNAD elements are provided in Appendix 1.

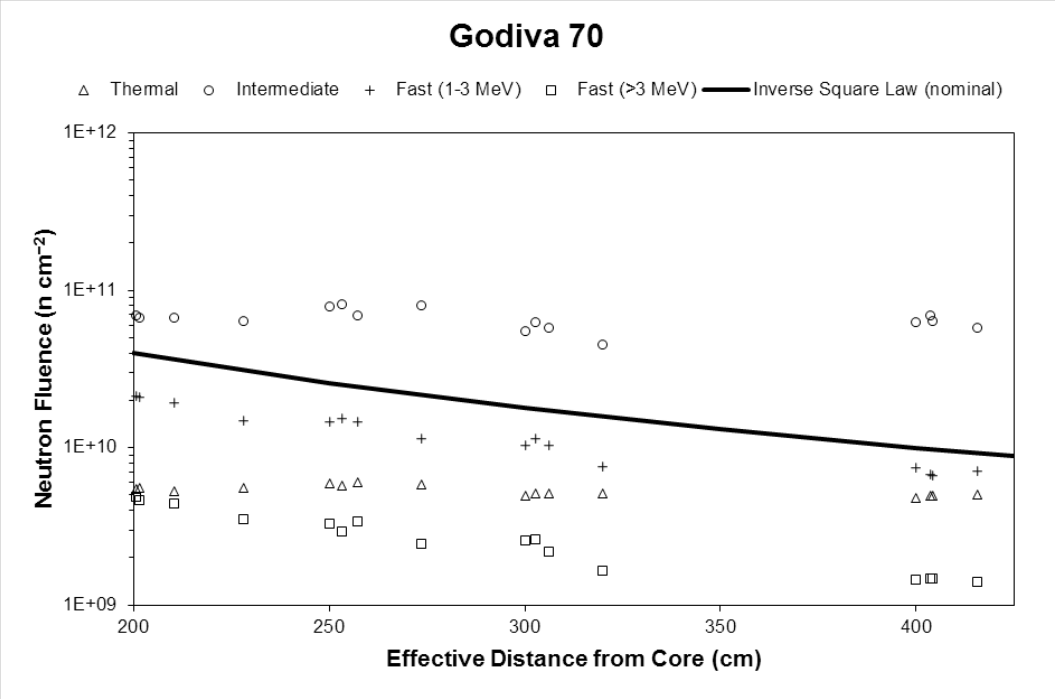

Figure 11. Average Neutron Fluence Results for Godiva 70

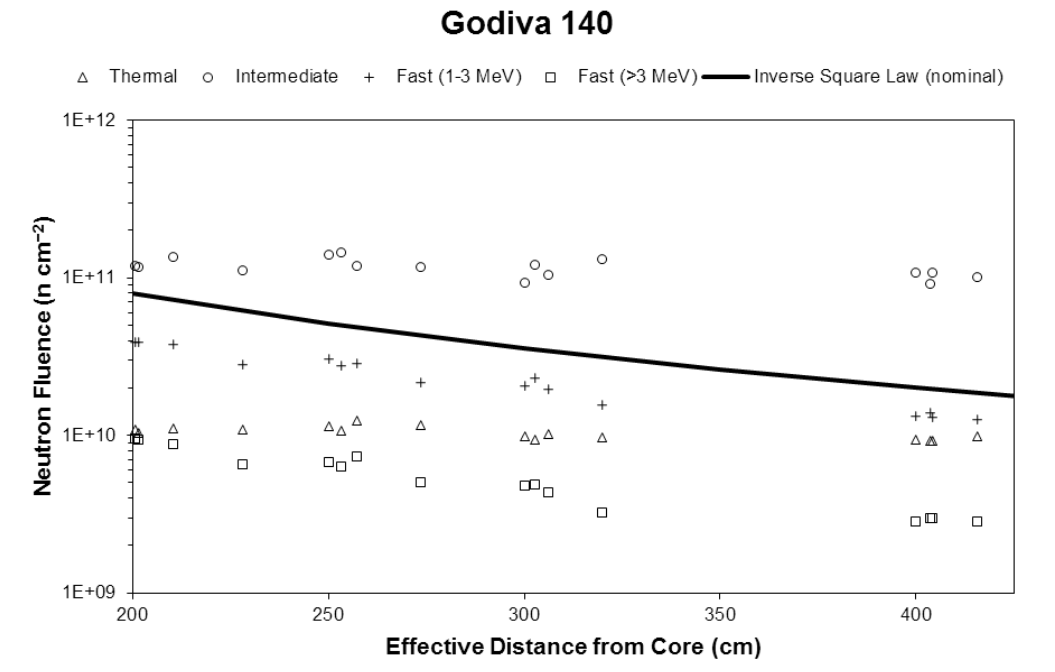

Figure 12. Average Neutron Fluence Results for Godiva 140

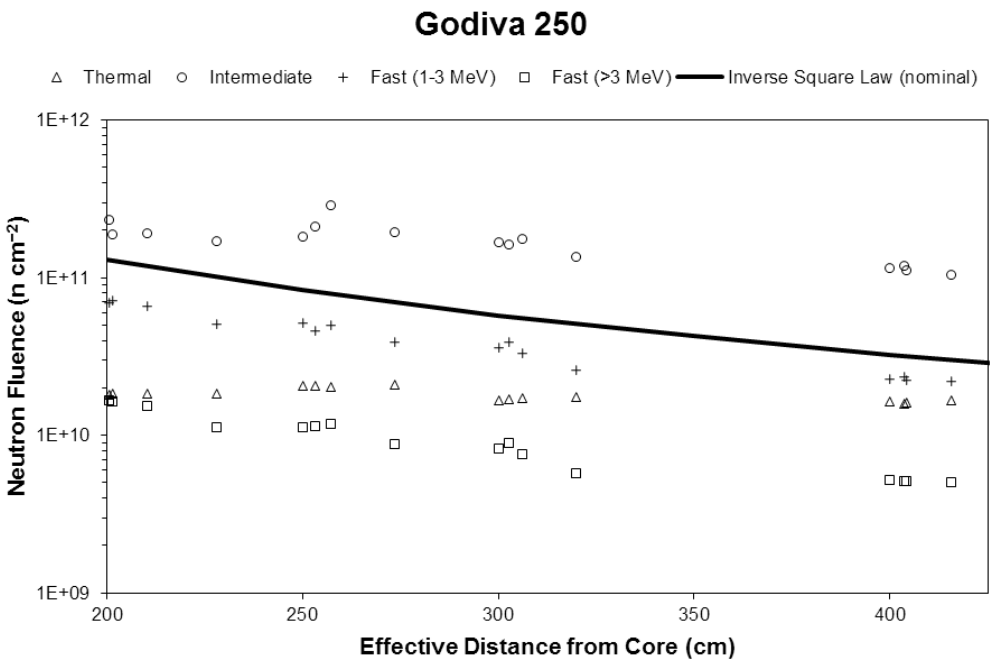

Figure 13. Average Neutron Fluence Results for Godiva 250

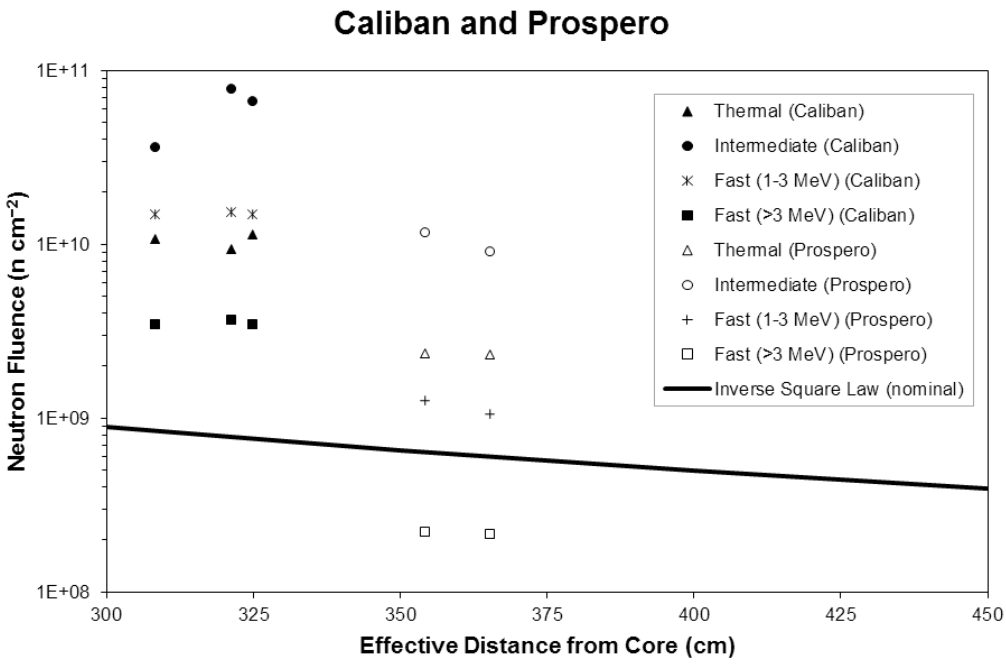

Figure 14. Average Neutron Fluence Results for Caliban and Prospero

The PNAD results demonstrate a fairly consistent distribution of neutron energies for each critical assembly. Figure 15 below shows the average distribution of neutron energies by critical assembly. In the Godiva irradiations, where many more dosimeters were available, the fast neutron fluence as measured by the PNADs is seen to decrease with increased distance from the reactor by a factor roughly corresponding to the inverse square law. For intermediate and thermal neutrons, the fluence decrease with distance is less pronounced due to scattering reactions in the facility.

In each case, intermediate neutrons (in this work, considered to be neutrons with energies from 1 eV to 1 MeV) accounted for over 65% of the total neutron fluence, and fast neutrons with energies greater than 3 MeV accounted for 4% or less of the total fluence.

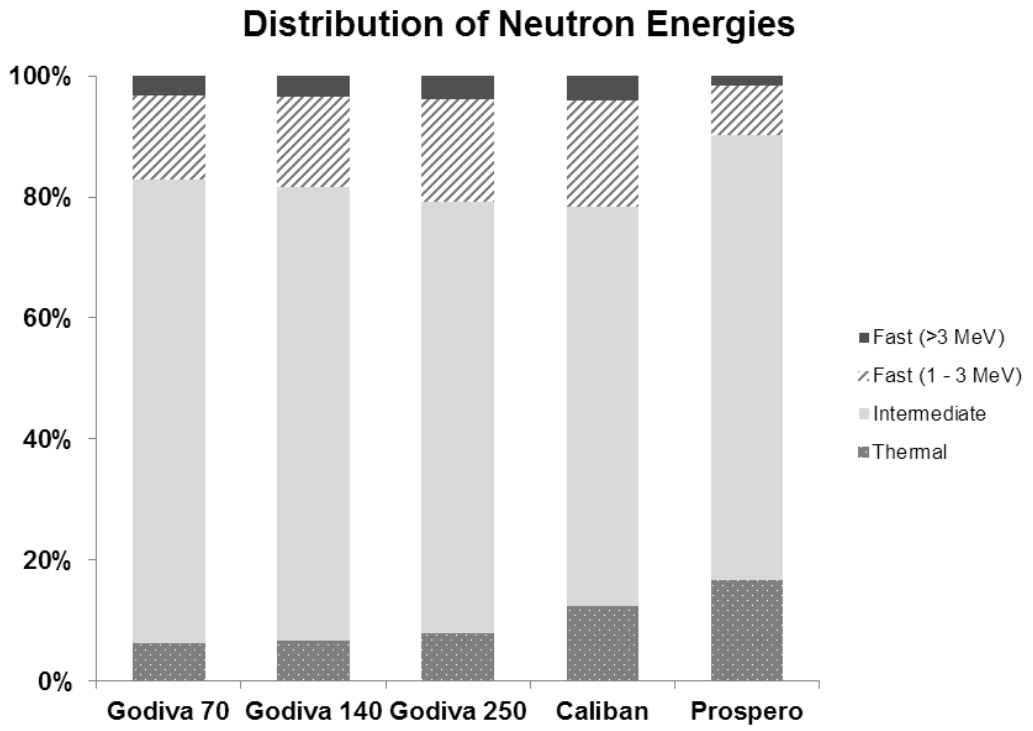

Figure 15. Average Distribution of Neutron Energies per Critical Assembly

3.1.2 DETERMINATION OF NEUTRON DOSE

The neutron fluence values determined from the measured activity of the neutron activation elements are further converted to dose using the fluence-to-dose conversion coefficients given in the LLNL technical basis document (LLNL 2012). These values were originally developed in 1984 using the calculated neutron leakage spectra from the bare and shielded Health Physics Research Reactor assembly at the Oak Ridge National Laboratory (Hankins 1984). The dose conversion coefficients are reproduced below in Table 5.

Table 5. Fluence-to-Dose Conversion Coefficients for LLNL PNAD Elements

Neutron Energy Range	Fluence-to-Dose Conversion Coefficient (Gy cm^2 n^{-1})
Thermal	7.0×10^{-15}
1 eV – 1 MeV	8.1×10^{-14}
1–3 MeV	3.3×10^{-13}
>3 MeV	5.3×10^{-13}

Figure 16 below shows the average distribution of neutron dose by critical assembly. In the Godiva and Caliban burst irradiations, the dose from neutrons with energies above 1 MeV accounted for 50–60% of the total neutron dose, while almost all of the remaining dose was due to intermediate neutrons (neutrons with energies from 1 eV to 1 MeV). In the steady-state Prospero irradiation, the fast neutron dose accounted for about 35% of the total neutron dose and the intermediate neutron dose accounted for about 60% of the total neutron dose. This difference is due to the softer neutron spectrum of the Prospero reactor in a steady-state mode compared to the burst irradiations using the Godiva and Caliban reactors.

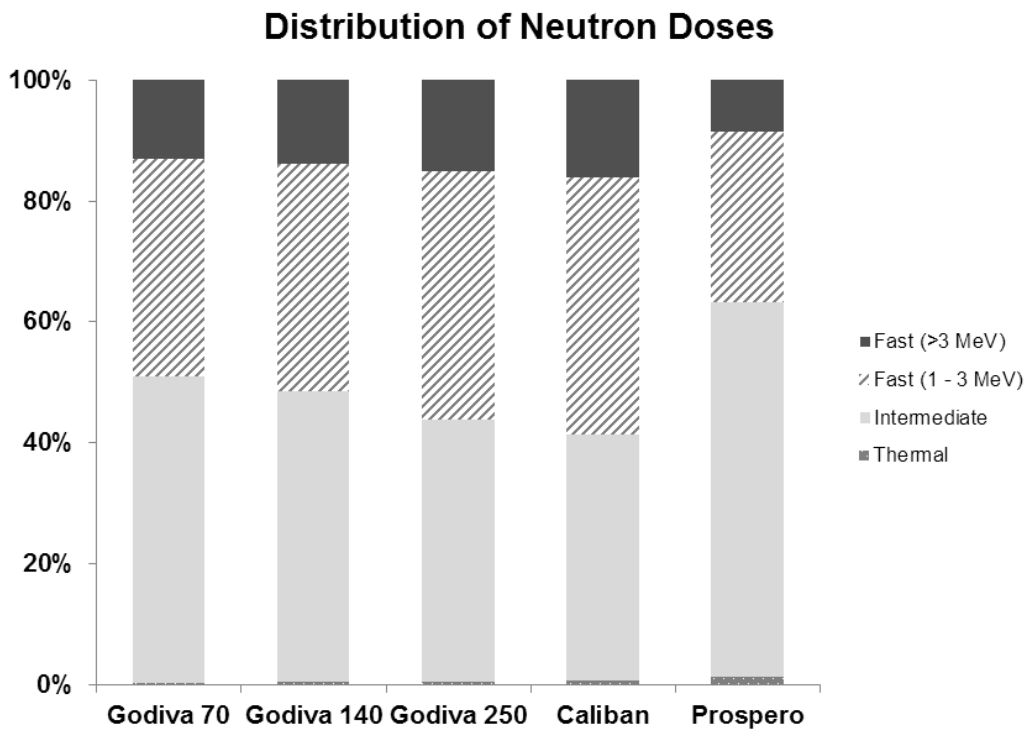

Figure 16. Average Distribution of Neutron Doses per Critical Assembly

3.2 CR-39 RESULTS

3.2.1 NEUTRON ENERGY THRESHOLD FOR CR-39

Data from the Godiva irradiations were used to confirm that the CR-39 foils are insensitive to thermal neutrons and part of the intermediate energy range of 1 eV to 1 MeV. Figures 17 and 18 show the CR-39 optical density results as a function of neutron fluence calculated using the collocated PNAD elements. Since the PNAD is capable of resolving a neutron spectrum to four energy regions, results for each region could be reviewed separately. Figure 17 shows that there is little correlation between thermal and intermediate neutron fluence and optical density. In contrast, Figure 18 shows good correlation between fast neutron fluence and optical density.

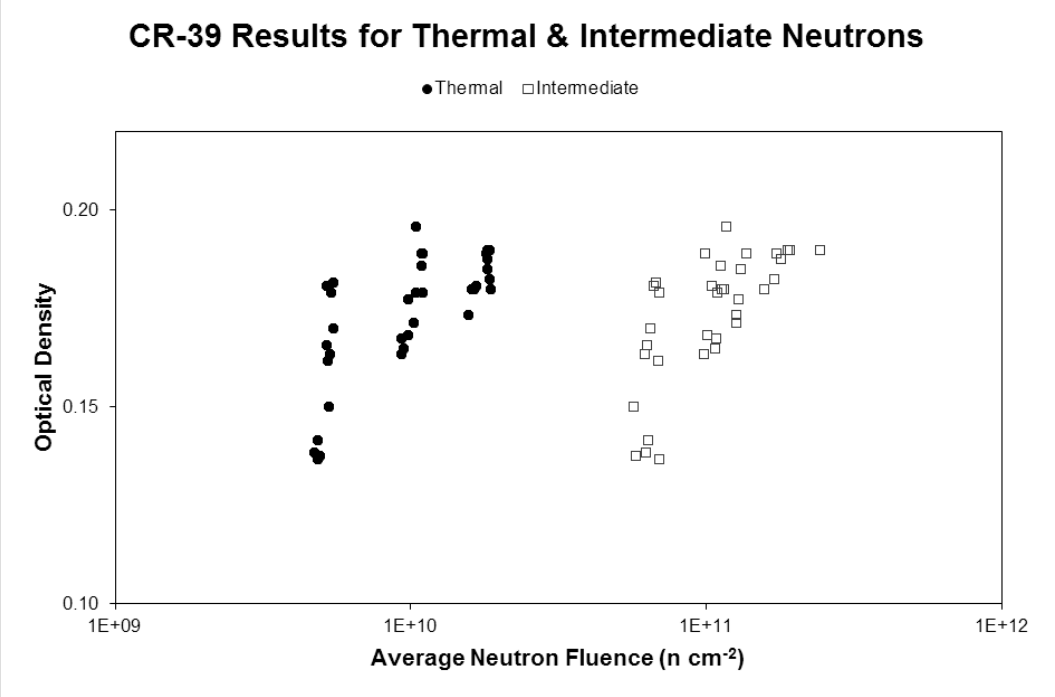

Figure 17. Optical Density as a Function of Thermal and Intermediate Neutron Fluence

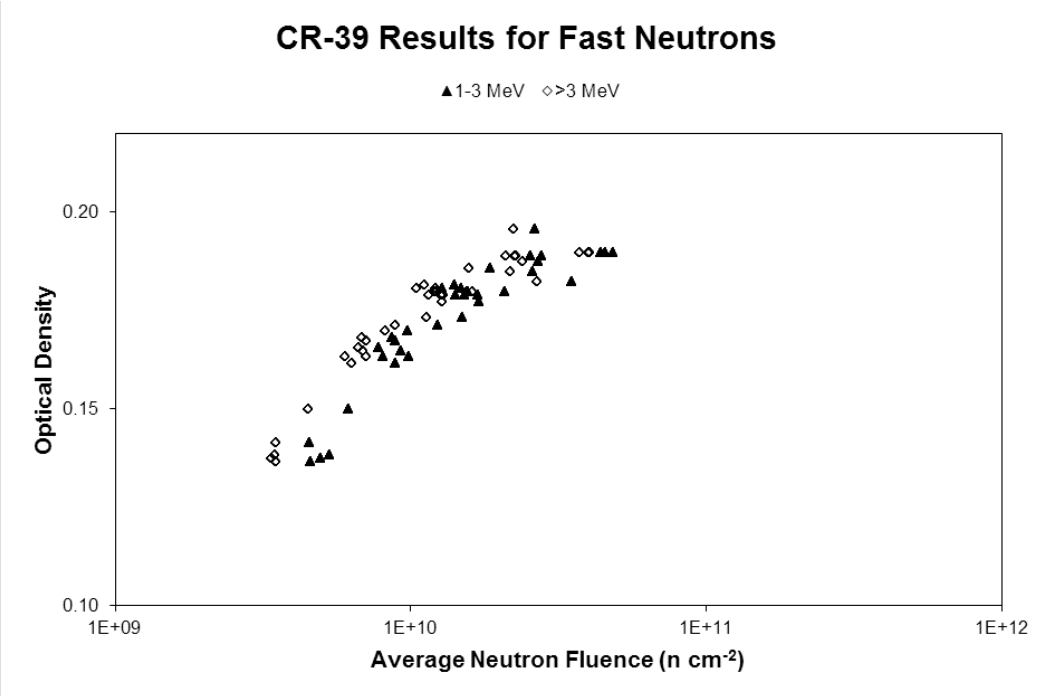

Figure 18. Optical Density as a Function of Fast Neutron Fluence

3.2.2 DETERMINATION OF OPTICAL DENSITY

The CR-39 results were averaged in groups according to their effective distance from the reactor core. In the Godiva irradiations, similar to the PNAD results for fast neutron fluence, the optical density decreases with increased distance from the reactor. However, it is evident that the relationship between optical density and distance from the reactor does not follow the inverse square law. The results of the optical density measurements of the CR-39 foils are shown in Figure 19. Detailed results of the CR-39 optical density measurements are provided in Appendix 2.

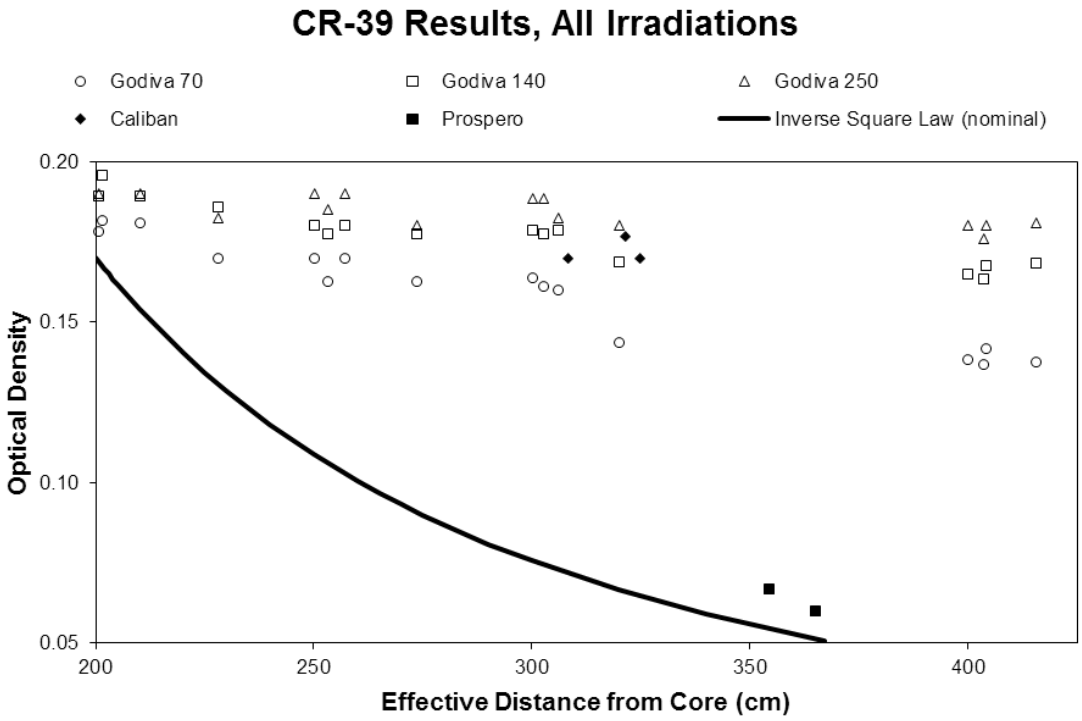

Figure 19. Average Optical Density Results for All Irradiations

4 DISCUSSION

4.1 EXPERIMENT DESIGN AND DATA SELECTION

The CR-39 foils were irradiated in large-scale experiments designed to fulfill multiple objectives, and not all results were relevant to present in this report. In particular, the Caliban and Prospero irradiations at the CEA Valduc facility studied PNAD response to varying configurations, including angular orientations and placement on sodium-water phantoms as well as aluminum stands. These irradiations were done with relatively small numbers of dosimeters (27 in the Caliban irradiation and 14 in the Prospero irradiation, compared to 144 dosimeters for each of the three Godiva irradiations). Due to the limited data available for the alternative configurations, the results for dosimeters placed on phantoms and at angular orientations are not presented in this report.

4.2 CORRELATION BETWEEN CR-39 OPTICAL DENSITY AND FAST NEUTRON FLUENCE AND DOSE

As previously discussed, CR-39 is insensitive to thermal neutrons and has a reaction threshold of approximately 100 keV. The LLNL PNAD design resolves a neutron spectrum fluence into four energy regions: thermal, intermediate (1 eV – 1 MeV), and fast (two regions, one between 1–3 MeV and another above 3 MeV). Since the PNAD covers a wider range of intermediate neutron energies (from 1 eV to 1 MeV) than CR-39, and the CR-39 does not differentiate between >1 MeV and >3 MeV neutrons, the CR-39 optical density results were compared to the total fast neutron fluence (>1 MeV).

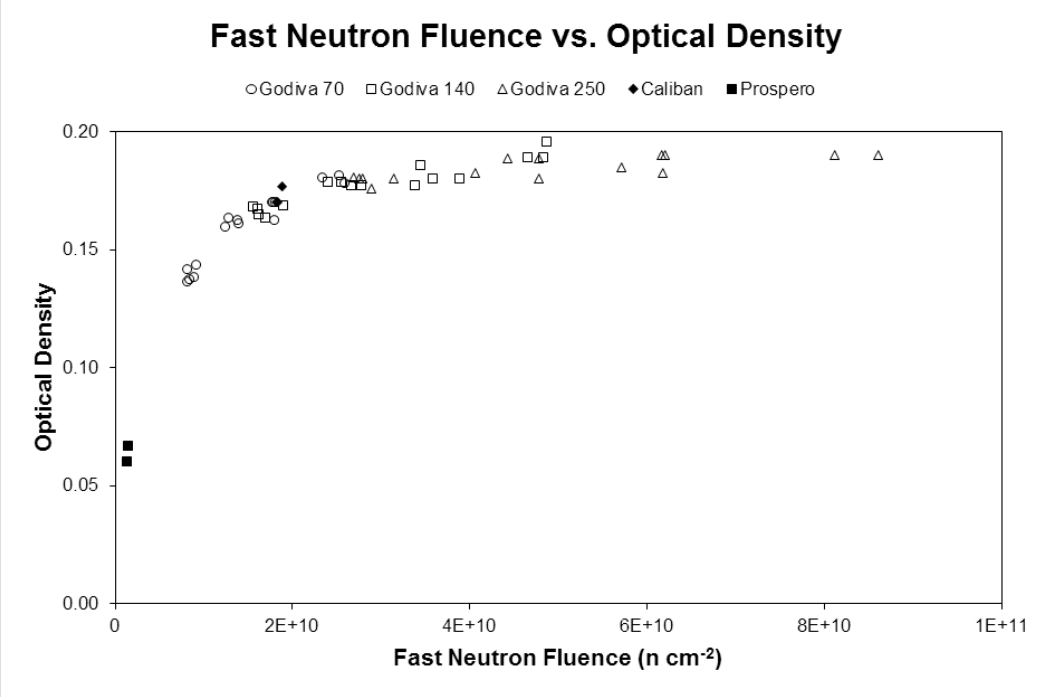

Figure 20. Average Optical Density Results as a Function of Fast Neutron Fluence

Figure 20 shows the average optical density results of the CR-39 foils in each irradiation for fast neutrons. The five irradiation experiments are differentiated in this figure, but the data demonstrate that each experiment is in good agreement with the overall trend. This plot also shows that optical density resulting from the etching procedure used in this work is not a linear function of fast neutron fluence, and therefore would not be expected to follow the inverse square law in decreasing with distance from the reactor. The fast neutron fluence was determined using the neutron activation elements as described in Section 3.1.1 above. From the fluence values, the absorbed dose was determined using the fluence-to-dose conversion coefficients described in Section 3.1.2.

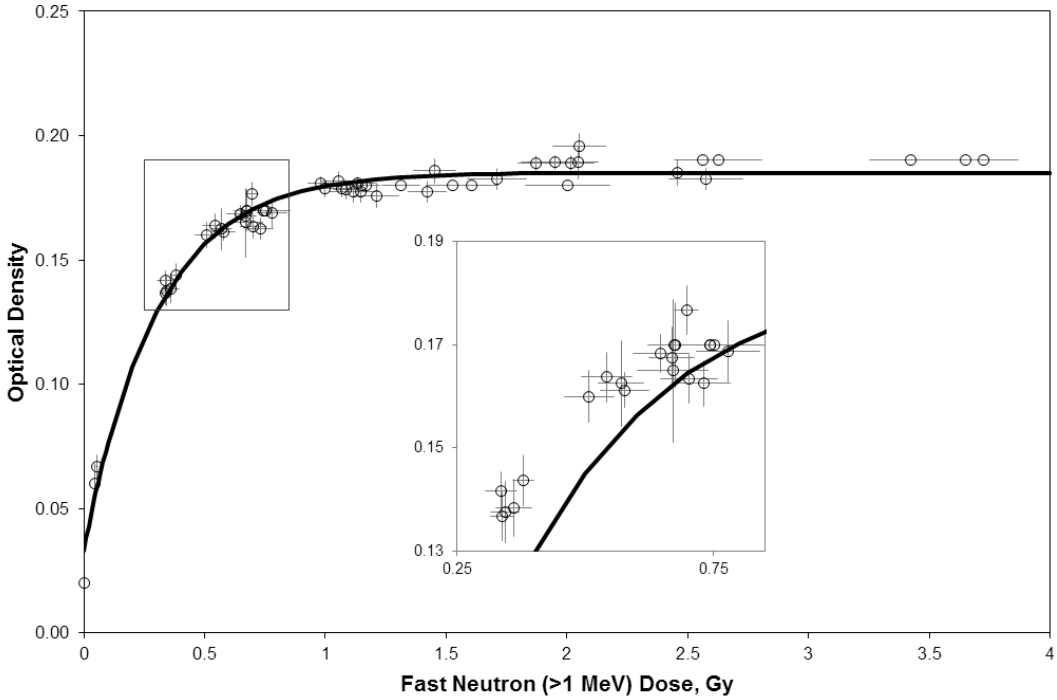

Figure 21. Optical Density of CR-39 as a Function of Fast Neutron Dose

The averaged absorbed dose results are plotted in Figure 21. Each marker represents a set of dosimeters in the same irradiation experiment with the same effective distance from the reactor core. The solid line shows an exponential fit to Equation 3 performed using the R programming language with the non-linear least squares regression "nls2" package, where *x* is the fast neutron absorbed dose in Gy.

$$y = a + be^{-cx} \qquad \text{Equation 3}$$

The "nls2" package was used to determine the weighted least-squares estimates for the parameters *a*, *b*, and *c*. These are shown in Equation 4:

$$\text{OD} = 0.185 - 0.152e^{-3.33x} \qquad \text{Equation 4}$$

Figure 21 shows that while there is a correlation between the optical density of CR-39 and the fast neutron dose measured using the PNAD neutron activation elements, the optical density measurements exhibit a definite point of saturation. A review of all measurements conducted for this work revealed that the measured optical density approaches a maximum value of 0.20 under the chemical etching conditions described in Section 2.3.1. The optical density saturation point is reached at a fast neutron absorbed dose of approximately 1 Gy.

5 CONCLUSION

This work demonstrates that CR-39 is a viable neutron dosimeter for high doses of fast neutrons (neutrons with energy greater than 1 MeV), such as those that could occur in a criticality accident. The optical density of CR-39 foils irradiated in nuclear accident dosimetry experiments can provide an independent verification of the fast neutron doses measured by neutron activation foils up to an absorbed dose of approximately 1 Gy. Optical density of chemically etched CR-39 foils was measured using a transmission densitometer and found to be an exponential function of the fast neutron dose measured by the neutron activation components of the nuclear accident dosimeters.

This work used the standard LLNL procedure for chemical etching of CR-39 neutron dosimeters. Further studies are warranted to enhance the dose range and optimize analysis of the CR-39 foils following high dose irradiations. One possibility is to study various light sources in the transmission densitometer, which could enhance the differences in optical density measurements. Another possibility for further study is to examine the potential for analysis of the CR-39 foils directly after irradiation, without chemical etching. Finally, the etching process itself should be studied to determine if it can be improved for optical density measurements rather than individual track analysis, as in the current etching procedure. Such studies could be valuable additions to dosimetry programs for nuclear criticality accidents and other high neutron dose situations.

REFERENCES

ANSI/HPS (2013). *Dosimetry for Criticality Accidents* (N13.3). McLean, VA: Health Physics Society.

Arneja, A. R., Waker, A. J. (1995). "Wide-Range Neutron Dose Determination with CR-39." *Radiation Protection Dosimetry*, Vol. 58, No. 3, p. 201–204.

Auxier, J. A., Snyder, W. S., Jones, T. D. (1968). "Neutron Interactions and Penetration in Tissue." In Attix, F. H. and Roesch, W. C. (Eds.), *Radiation Dosimetry: Volume I, Fundamentals*, Second Edition. Academic Press, New York.

Bordy, J., Médioni, R., Portal, G. (1991). "Spectrophotometric Measurement of Track Density in CR39 for High Neutron Dose Determinations." *Nuclear Tracks and Radiation Measurements*, Vol. 19, No. 1–4, p. 241–244.

Casoli, P., Authier, N., Jacquet, X., Cartier, J. (2014). "Characterization of the Caliban and Prospero Critical Assemblies Neutron Spectra for Integral Measurements Experiments." *Nuclear Data Sheets*, Vol. 118, p. 554–557.

Castillo, F., Espinosa, J., Golzarri, J. I., et al. (2013). "Fast neutron dosimetry using CR-39 track detectors with polyethylene as radiator." *Radiation Measurements*, Vol. 50, p. 71–73.

Pinfold, J. L. (2012). "The MoEDAL Experiment at the LHC." In S. Giani, C. Leroy, L. Price, P. G. Rancoita, & R. Ruchti (Eds.), *Astroparticle, Particle, Space Physics and Detectors for Physics Applications*. Paper presented at the 13th ICATPP Conference, Como, Italy, 3–7 October 2011(p. 515–524). Singapore, World Scientific Publishing Co. Pte. Ltd.

Goda, J., Hayes, D., Sanchez, R (2013). "Godiva IV Critical Assembly Machine Reassembly and Startup." *Transactions of the American Nuclear Society*, Vol. 109, p. 893–896.

Griffith, R. V. (1973). "Use of ^{10}B-Loaded Plastic in Personnel Neutron Dosimetry." In *Volume II, Neutron Monitoring for Radiation Protection Purposes, Proceedings of a Symposium, Vienna, 11-15 December 1972*. Vienna, Austria. IAEA-SM-167/62.

Grothendieck, G. (2013). nls2: Non-linear regression with brute force. R Package version 0.2. ***https://CRAN.R-project.org/package=nls2***.

REFERENCES (Continued)

Hankins, D. E. (1984). "A Nuclear Accident Dosimeter Designed for Use with the Panasonic TLD System." In Griffith, R. V. (Ed.), *Hazards Control Department Annual Technology Review*. UCRL-50007-84.

Hankins, D. E., Homann, S. G., Buddemeier, B. (1989). *Personnel Neutron Dosimetry Using Electrochemically Etched CR-39 Foils, Revision 1*. UCRL-53833 Rev. 1.

Heinrichs, D. P., et al. (2014). *Final Design for an International Intercomparison Exercise for Nuclear Accident Dosimetry at the DAF Using GODIVA-IV*. LLNL-TR-661851.

International Commission on Radiological Protection (1996). *Conversion Coefficients for use in Radiological Protection against External Radiation*. ICRP Publication 74. Ann. ICRP 26 (3–4).

Knoll, G. F. (2000). *Radiation Detection and Measurement* (3rd ed.). New York, NY: John Wiley & Sons, Inc.

LLNL (2012). *Lawrence Livermore National Laboratory's Nuclear Criticality Accident System: Technical Basis*. (LLNL internal document.)

Lobaugh, M. L., Hickman, D. P., Wong, C. W., Wysong, A. R., Merritt, M. J., Heinrichs, D. P., Topper, J. D. (2015). *LLNL Results from CALIBAN-PROSPERO Nuclear Accident Dosimetry Experiments in September 2014*. LLNL-TR-671548.

Myers, W. L., Bounds, J. A., Clement, S. D., Dinwiddie, D. R., Goda, J. M., Hayes, D. K., Sanchez, R. G. (2010). "Criticality Experiment Capabilities Located at the Nevada Test Site." *Transactions of the American Nuclear Society*, Vol. 103, p. 401–402.

Occupational Radiation Protection, 10 C.F.R. § 835 (2016).

R Core Team (2016). R: A language and environment for statistical computing. R Foundation for Statistical Computing, Vienna, Austria. URL ***https://www.R-project.org***.

Radev, R. (2009). *Characterization of the Neutron Fields in the Lawrence Livermore National Laboratory (LLNL) Radiation Calibration Laboratory Low Scatter Calibration Facility*. LLNL-TR-416791.

REFERENCES (Continued)

Sahoo, G. S., Tripathy, S. P., Paul, S., Sharma, S. C., Joshi, D. S., Gupta, A. K., Bandyopadhyay, T. (2015). "Effects of high neutron doses and duration of the chemical etching on the optical properties of CR-39." *Applied Radiation and Isotopes*, Vol. 101, p. 114–121.

Topper, J. (2016). *LLNL External Dosimetry QA Manual Procedures and Technical Basis Documents*. LLNL-TM-686335.

Turner, J. E. (2007). *Atoms, Radiation, and Radiation Protection* (3rd ed.). Weinheim, Germany: Wiley-VCH Verlag GmbH & Co. KGaA.

Yasuda, N., Koguchi, Y., Tsubomatsu, M., Takagi, Tl, Kobayashi, Il, Tsuruta, T., Morishima, H. (2006). "Extremely high dose neutron dosimetry using CR-39 and atomic force microscopy." *Radiation Protection Dosimetry*, Vol. 120, No. 1–4, p. 470–474.

APPENDICES

APPENDIX 1

PNAD DATA

Table 6. Average PNAD Results for Godiva 70

Effective Distance (cm)	Number of PNADs	Average Thermal Neutron Fluence (n cm^{-2})	Average Intermediate (1 eV – 1 MeV) Neutron Fluence (n cm^{-2})	Average Fast (1 – 3 MeV) Neutron Fluence (n cm^{-2})	Average Fast (>3 MeV) Neutron Fluence (n cm^{-2})
200.7	12	5.37E+09	6.94E+10	2.09E+10	4.87E+09
201.4	12	5.46E+09	6.72E+10	2.07E+10	4.66E+09
210.3	12	5.19E+09	6.70E+10	1.89E+10	4.45E+09
228.0	12	5.46E+09	6.34E+10	1.46E+10	3.49E+09
250.2	4	5.83E+09	7.84E+10	1.45E+10	3.29E+09
253.2	4	5.63E+09	8.13E+10	1.50E+10	2.93E+09
257.2	4	5.95E+09	6.98E+10	1.43E+10	3.42E+09
273.5	4	5.73E+09	8.04E+10	1.13E+10	2.46E+09
300.2	8	4.87E+09	5.50E+10	1.02E+10	2.55E+09
302.7	8	5.02E+09	6.26E+10	1.13E+10	2.59E+09
306.0	8	5.01E+09	5.78E+10	1.02E+10	2.17E+09
319.9	8	5.06E+09	4.51E+10	7.51E+09	1.65E+09
400.0	12	4.71E+09	6.25E+10	7.32E+09	1.46E+09
403.6	12	4.83E+09	6.91E+10	6.66E+09	1.46E+09
404.0	12	4.84E+09	6.34E+10	6.59E+09	1.48E+09
415.5	12	4.92E+09	5.75E+10	6.96E+09	1.41E+09

Table 7. Average PNAD Results for Godiva 140

Effective Distance (cm)	Number of PNADs	Average Thermal Neutron Fluence (n cm^{-2})	Average Intermediate (1 eV – 1 MeV) Neutron Fluence (n cm^{-2})	Average Fast (1 – 3 MeV) Neutron Fluence (n cm^{-2})	Average Fast (>3 MeV) Neutron Fluence (n cm^{-2})
200.7	12	1.09E+10	1.19E+11	3.88E+10	9.46E+09
201.4	12	1.04E+10	1.17E+11	3.93E+10	9.35E+09
210.3	12	1.10E+10	1.36E+11	3.77E+10	8.73E+09
228.0	12	1.09E+10	1.11E+11	2.79E+10	6.53E+09
250.2	4	1.15E+10	1.40E+11	3.04E+10	6.71E+09
253.2	4	1.08E+10	1.45E+11	2.75E+10	6.35E+09
257.2	4	1.25E+10	1.18E+11	2.85E+10	7.28E+09
273.5	4	1.17E+10	1.17E+11	2.15E+10	5.07E+09
300.2	8	9.81E+09	9.28E+10	2.07E+10	4.83E+09
302.7	8	9.34E+09	1.21E+11	2.30E+10	4.85E+09
306.0	8	1.02E+10	1.04E+11	1.96E+10	4.34E+09
319.9	8	9.66E+09	1.31E+11	1.56E+10	3.24E+09
400.0	12	9.45E+09	1.07E+11	1.33E+10	2.85E+09
403.6	12	9.27E+09	9.18E+10	1.40E+10	2.98E+09
404.0	12	9.28E+09	1.08E+11	1.30E+10	2.96E+09
415.5	12	9.79E+09	1.00E+11	1.27E+10	2.84E+09

Table 8. Average PNAD Results for Godiva 250

Effective Distance (cm)	Number of PNADs	Average Thermal Neutron Fluence (n cm^{-2})	Average Intermediate (1 eV – 1 MeV) Neutron Fluence (n cm^{-2})	Average Fast (1 – 3 MeV) Neutron Fluence (n cm^{-2})	Average Fast (>3 MeV) Neutron Fluence (n cm^{-2})
200.7	12	1.81E+10	2.34E+11	6.96E+10	1.65E+10
201.4	12	1.83E+10	1.88E+11	7.21E+10	1.64E+10
210.3	12	1.84E+10	1.92E+11	6.59E+10	1.52E+10
228.0	12	1.84E+10	1.69E+11	5.06E+10	1.11E+10
250.2	4	2.06E+10	1.81E+11	5.16E+10	1.13E+10
253.2	4	2.05E+10	2.13E+11	4.56E+10	1.15E+10
257.2	4	2.01E+10	2.90E+11	5.03E+10	1.18E+10
273.5	4	2.09E+10	1.96E+11	3.91E+10	8.85E+09
300.2	8	1.66E+10	1.67E+11	3.60E+10	8.28E+09
302.7	8	1.70E+10	1.61E+11	3.90E+10	8.92E+09
306.0	8	1.71E+10	1.77E+11	3.32E+10	7.57E+09
319.9	8	1.76E+10	1.37E+11	2.58E+10	5.71E+09
400.0	12	1.63E+10	1.15E+11	2.27E+10	5.18E+09
403.6	11	1.58E+10	1.19E+11	2.36E+10	5.13E+09
404.0	12	1.61E+10	1.11E+11	2.25E+10	5.10E+09
415.5	12	1.67E+10	1.05E+11	2.20E+10	5.07E+09

Table 9. Average PNAD Results for Caliban Irradiation

Effective Distance (cm)	Number of PNADs	Average Thermal Neutron Fluence (n cm^{-2})	Average Intermediate (1 eV – 1 MeV) Neutron Fluence (n cm^{-2})	Average Fast (1 – 3 MeV) Neutron Fluence (n cm^{-2})	Average Fast (>3 MeV) Neutron Fluence (n cm^{-2})
308.2	3	1.08E+10	3.60E+10	1.49E+10	3.45E+09
321.3	3	9.41E+09	7.90E+10	1.52E+10	3.70E+09
324.8	3	1.14E+10	6.70E+10	1.49E+10	3.48E+09

Table 10. Average PNAD Results for Prospero Irradiation

Effective Distance (cm)	Number of PNADs	Average Thermal Neutron Fluence (n cm^{-2})	Average Intermediate (1 eV – 1 MeV) Neutron Fluence (n cm^{-2})	Average Fast (1 – 3 MeV) Neutron Fluence (n cm^{-2})	Average Fast (>3 MeV) Neutron Fluence (n cm^{-2})
354.3	3	2.37E+09	1.18E+10	1.26E+09	2.23E+08
365.2	3	2.33E+09	9.16E+09	1.06E+09	2.16E+08

APPENDIX 2

CR-39 DATA

Table 11. Average CR-39 Results for Godiva 70

Radial Distance (m)	Height (cm)	Effective Distance (cm)	Number of CR-39 Foils	Average OD	Standard Deviation
2	197	200.7	11	0.178	0.0039
2	156	201.4	12	0.182	0.0037
2	115	210.3	12	0.181	0.0028
2	70.5	228.0	12	0.170	0.0000
2.5	169.5	250.2	4	0.170	0.0000
2.5	220	253.2	4	0.163	0.0043
2.5	119.5	257.2	4	0.170	0.0000
2.5	69	273.5	4	0.163	0.0083
3	169.5	300.2	8	0.164	0.0048
3	220	302.7	8	0.161	0.0033
3	119.5	306.0	8	0.160	0.0050
3	69	319.9	8	0.144	0.0048
4	178.5	400.0	12	0.138	0.0055
4	234	403.6	12	0.137	0.0047
4	123	404.0	12	0.142	0.0037
4	67.5	415.5	12	0.138	0.0060

Table 12. Average CR-39 results for Godiva 140

Radial Distance (m)	Height (cm)	Effective Distance (cm)	Number of CR-39 Foils	Average OD	Standard Deviation
2	197	200.7	12	0.189	0.0064
2	156	201.4	12	0.196	0.0049
2	115	210.3	12	0.189	0.0028
2	70.5	228.0	12	0.186	0.0049
2.5	169.5	250.2	4	0.180	0.0000
2.5	220	253.2	4	0.178	0.0043
2.5	119.5	257.2	4	0.180	0.0000
2.5	69	273.5	4	0.178	0.0043
3	169.5	300.2	8	0.179	0.0033
3	220	302.7	8	0.178	0.0043
3	119.5	306.0	8	0.179	0.0033
3	69	319.9	8	0.169	0.0060
4	178.5	400.0	12	0.165	0.0138
4	234	403.6	12	0.163	0.0060
4	123	404.0	12	0.168	0.0060
4	67.5	415.5	12	0.168	0.0037

Table 13. Average CR-39 results for Godiva 250

Radial Distance (m)	Height (cm)	Effective Distance (cm)	Number of CR-39 Foils	Average OD	Standard Deviation
2	197	200.7	12	0.190	0.0000
2	156	201.4	12	0.190	0.0000
2	115	210.3	12	0.190	0.0000
2	70.5	228.0	12	0.183	0.0043
2.5	169.5	250.2	3	0.190	0.0000
2.5	220	253.2	4	0.185	0.0050
2.5	119.5	257.2	4	0.190	0.0000
2.5	69	273.5	4	0.180	0.0000
3	169.5	300.2	8	0.189	0.0033
3	220	302.7	8	0.189	0.0033
3	119.5	306.0	8	0.183	0.0043
3	69	319.9	8	0.180	0.0000
4	178.5	400.0	12	0.180	0.0000
4	234	403.6	12	0.176	0.0049
4	123	404.0	12	0.180	0.0000
4	67.5	415.5	12	0.181	0.0028

Table 14. Average CR-39 Results for Caliban Irradiation

Radial Distance (m)	Height (cm)	Effective Distance (cm)	Number of CR-39 Foils	Average OD	Standard Deviation
3	95.6	308.2	3	0.170	0.0000
3	140	321.3	3	0.177	0.0047
3	149.5	324.8	3	0.170	0.0082

Table 15. Average CR-39 Results for Prospero Irradiation

Radial Distance (m)	Height (cm)	Effective Distance (cm)	Number of CR-39 Foils	Average OD	Standard Deviation
3.5	90.1	354.3	3	0.067	0.0047
3.5	139.3	365.1	3	0.060	0.0082